agriculture

MDPI

Article

Prediction Models for Non-Destructive Identification of Compacted Soil Layers Based on Electrical Conductivity and Moisture Content

Hasan Mirzakhaninafchi [1,*], Ahmet Celik [2], Roaf Parray [3] and Abir Mohammad Hadi [4]

[1] College of Engineering, University of Georgia, Tifton, GA 31793, USA
[2] Department of Agricultural Machinery and Technologies Engineering, Faculty of Agriculture, Atatürk University, Erzurum 25240, Turkey; ahcelik@atauni.edu.tr
[3] Division of Agricultural Engineering, Indian Council of Agricultural Research–Indian Agricultural Research Institute (ICAR–IARI), New Delhi 110012, India; rouf.engg@gmail.com
[4] Computer Science and Software Engineering, School of Computing and Analytics, College of Informatics, Northern Kentucky University, Highland Heights, KY 41099, USA; hadia1@nku.edu
* Correspondence: hasan.mirzakhaninafchi@uga.edu

Abstract

Crop root development, and in turn crop growth, is strongly influenced by soil strength and the mechanical impedance of compacted layers, which restrict root elongation and exploration. Because the depth and thickness of compacted layers vary across a field, their identification is essential for site-specific tillage and sustainable root-zone management. A sensing approach that can support future real-time identification of compacted layers after soil-specific calibration, which would enable variable-depth tillage, reducing mechanical impedance and improving energy-use efficiency while maintaining crop yields. This study aimed to develop and evaluate prediction models that can support future real-time identification of compacted soil layers using soil electrical conductivity (EC) and moisture content as non-destructive indicators. A sandy clay soil (48.6% sand, 29.3% clay, 22.1% silt) was tested in a soil-bin laboratory under controlled conditions at three moisture levels (13, 18, and 22% db.) and six depth layers (C1–C6, 0–30 cm) identified from the penetration-resistance profile to measure penetration resistance, shear resistance, and EC. Penetration and shear resistance increased toward the most resistant depth layer and decreased with increasing moisture content, whereas EC generally increased with both depth layer and moisture content. Linear regression models relating penetration resistance ($R^2 = 0.893$) and shear resistance ($R^2 = 0.782$) to EC and moisture content were developed and evaluated. Field validation in a paddy field of similar texture showed that predicted penetration resistance differed from measured values by 3–6% across the three compaction treatments evaluated. Root length density and root volume decreased with increasing machine-induced compaction, confirming the agronomic relevance of the modeled patterns and supporting the suitability of the proposed indicators. Together, these results demonstrate that EC and moisture content can potentially be used as non-destructive proxies for compacted-layer identification and provide a calibration basis for future on-the-go sensing systems to support site-specific, variable-depth tillage in agricultural fields.

Keywords: soil electrical conductivity; soil moisture content; penetration resistance; shear resistance; soil compaction; non-destructive sensing; predictive modeling; machine learning; variable-depth tillage; precision agriculture

Check for updates

Academic Editor: Ezio Riggi

Received: 7 December 2025
Revised: 5 January 2026
Accepted: 9 January 2026
Published: 13 January 2026

Copyright: © 2026 by the authors. Licensee MDPI, Basel, Switzerland. This article is an open access article distributed under the terms and conditions of the Creative Commons Attribution (CC BY) license.

1. Introduction

Global food demand is projected to increase substantially by 2050, and several studies suggest that, under current trajectories, yield growth will be insufficient to meet this demand without significant changes in how we manage soils and cropping systems [1]. Simply expanding the cropped area is neither environmentally nor economically sustainable. Instead, sustainable intensification—through precision farming and climate-smart, resource-efficient practices—is critical for maintaining productivity while limiting environmental damage [2,3]. Precision agriculture aims to match inputs and management decisions to the spatial and temporal variability of soil and crop conditions, thereby improving yield, energy-use efficiency, and profitability while reducing negative environmental impacts [4–6]. Improving the diagnosis and management of soil physical constraints is central to these goals.

A central barrier to sustainable intensification is soil compaction. Soil compaction increases bulk density and reduces pore volume by forcing soil particles into closer contact [7]. This alters pore-size distribution, mechanical properties, and the movement of water and gases [8–12]. As pores become smaller and less connected, root access to oxygen, water, and nutrients is restricted, leading to reduced root elongation, impaired shoot growth, and lower yield [13–19]. Compacted layers (hardpans) also promote surface runoff and erosion, and can increase the risk of environmental contamination by slowing the drainage of water carrying fertilizers and pesticides [20–24]. Consequently, practical tools for detecting compaction are important for both productivity and environmental stewardship.

Mechanical impedance experienced by roots is strongly affected by both soil moisture and soil strength. Drier soils typically exhibit higher penetration resistance and shear strength, which can severely limit root growth and increase crop vulnerability to drought [21,25–28]. Numerous studies have shown that soil bulk density, water content, texture, and depth all influence penetration resistance and shear resistance, and that these properties can be used to predict soil strength [29–37]. However, operational decisions in the field are still often made using fixed-depth tillage, regardless of the actual depth and thickness of compacted layers, leading to suboptimal energy use.

In many coastal plain and similar soils, hardpan depth shows substantial spatial variation [38,39]. Conventional fixed-depth subsoiling across the whole field can either fail to fully break the compacted layer or overpenetrate well below the hardpan. Overtillage increases draft requirements and fuel consumption and may disturb subsoil clay layers without yield benefit. Studies have reported that subsoiling deeper than necessary can increase draft and fuel use by 50–75% without improving crop productivity [40–42]. Prescription maps derived from cone index measurements suggest that a sizeable fraction of fields require less-than-maximum tillage depth to fracture the hardpan [38,43]. These findings highlight the potential of site-specific, variable-depth tillage to improve energy efficiency and protect soil structure [44–46]. Achieving this in practice requires reliable, spatially resolved detection of compacted layers.

A prerequisite for variable-depth tillage is the ability to identify the position of compacted layers in real time in the field. Soil penetration resistance and shear strength are well-established indices of soil mechanical status, but traditional measurements are discrete, slow, and labor-intensive [47–49]. In parallel, apparent soil electrical conductivity (EC) and electrical resistivity have been widely used as indirect indicators of soil properties such as texture, salinity, organic matter, and moisture content, and for delineating management zones [50–57]. Several studies have reported relationships between EC or resistivity and compaction-related properties, including bulk density and penetration resistance [58–63]. However, the direct coupling between EC, moisture content, and mechanical indices of soil

strength in compacted layers remains insufficiently quantified, especially under controlled conditions and with models aimed at real-time implementation for field operations.

In this context, the novelty of the present study is threefold: (i) it treats naturally occurring, depth-defined compaction strata in a sandy clay soil as an explicit framework for linking EC and moisture to two mechanical indices (penetration resistance and shear resistance) under controlled soil-bin conditions; (ii) it provides simple two-predictor linear calibration models (EC and moisture) for estimating both penetration resistance and shear resistance across the identified depth layers; and (iii) it performs a limited field consistency check in a paddy soil of similar texture using penetration resistance measurements and root-system responses to machine-induced compaction. The intended contribution is therefore a soil-specific calibration proof-of-concept, rather than a deployable on-the-go sensing system.

Therefore, the overarching goal of this study was to develop and evaluate prediction models that can support future real-time identification (after soil-specific calibration) of soil compacted layers using soil electrical conductivity and moisture content. Specifically, the objectives were to: (i) quantify the relationships among soil penetration resistance, shear resistance, EC, and moisture content across six depth layers (C1–C6) and three moisture levels in a sandy clay soil under controlled soil-bin conditions; (ii) derive regression models that predict penetration resistance and shear resistance from EC and moisture content; and (iii) validate the predictive approach under field conditions using root system measurements and explore the relative importance of the input variables using interpretable machine learning techniques. The ultimate aim is to provide a basis for sensor development to support on-the-go, site-specific variable-depth tillage and to reduce unnecessary energy use while maintaining soil health and crop productivity.

2. Materials and Methods

2.1. Description of the Soil Bin

The study was conducted under controlled conditions in the soil-bin laboratory at the Department of Agricultural Machinery and Technology Engineering, Faculty of Agriculture, Ataturk University (Figure 1). The soil bin provides a uniform and repeatable environment compared with field conditions, enabling controlled evaluation of depth-structured soil mechanical resistance and sensor measurements. The soil bin dimensions were 16 m long, 2.5 m wide, and 0.8 m deep, with an effective experimental length of 12 m. The soil texture in the bin was sandy clay (48.6% sand, 29.3% clay, and 22.1% silt).

2.2. Description of Instrumentation Tools Used in This Study

The experiment was conducted using an analog hand-pushed penetrometer (Eijkelkamp Hand penetrometer, Royal Eijkelkamp, Giesbeek, Netherlands) to determine soil penetration resistance; a soil shear resistance tester (Hand Vane Tester H-60, Geonor AS, Oslo, Norway) to determine soil shear resistance; a soil EC sensor (HI98331 Soil Test™ direct soil EC Tester, Hanna Instruments, Woonsocket, RI, USA) to determine the electrical conductivity of soil; and a soil moisture meter (Field Scout TDR 300, Spectrum Technologies Inc., Aurora, IL, USA) to determine soil moisture content.

2.2.1. Measurement of Soil Penetration Resistance

Soil penetration resistance is the force needed to push a probe tip into the soil [64,65]. An analog gauge Eijkelkamp penetrometer with a cone angle of 60° was used to measure soil penetration resistance in the present study. The cone on the shaft of the penetrometer was divided into 5 cm segments and could be pushed to a depth of 100 cm with 50 cm length extension shafts. The cone base area of the penetrometer was 1 cm^2 and its accuracy

was 1%, with an analog gauge of 0–1 kN. Since the experiment was carried out on no-till soil, a cone tip with a diameter of 11.28 mm was used in accordance with ASAE standard S313.3 [66]. The experiment was conducted by measuring soil penetration resistance at depths of up to 30 cm at 5 cm intervals with three replications of each interval from each plot. The penetrometer was inserted vertically at an approximately constant rate of ~3 cm s^{-1}, and penetration resistance was recorded at 5 cm depth increments to a depth of 30 cm [33,67–71]. To minimize operator-induced variability, the same trained operator performed all insertions, maintaining a steady insertion rate as consistently as possible. The values were read in kN, converted to kN/cm^2 by dividing by the cone area, and then expressed in MPa.

Figure 1. Soil bin laboratory.

2.2.2. Measurement of Soil Shear Resistance

The resistance of soil to deformation in the horizontal direction by an operation of shear (tangential) stress is known as soil shear resistance [47]. The shear resistance is influenced by two elements: soil internal friction angle and soil cohesion. They are usually determined from Mohr–Coulomb's standard, and can be denoted as follows:

$$\tau_f = c + \sigma_n \tan\phi \quad (1)$$

wherein ϕ, is the internal friction angle; c, is the cohesion; σ_n is the regular stress to the soil failure; and τ_f is the shear resistance [72].

In this experiment, the strength of soil to withstand shear stress was determined using a bladed soil shear resistance tester. The tool had three blades with fixed gaps and heights of 16 × 32 mm. Shear resistance measurements could be made at up to 300 cm with 50 cm long extension shafts and in the ranges of 0–260 kPa. The soil shear resistance tester was immersed in the soil to the desired measurement depth at which the measurement was made. The tool was manually rotated at an approximately constant angular velocity of ~5° s^{-1} (corresponding to one full revolution in approximately 36 s), following a slow shear test protocol. Although exact angular velocity control is not possible under manual operation, the same trained operator performed all measurements using a consistent rotation rate across all treatments. The data was read as kPa with 10% sensitivity [48,49,73].

2.2.3. Measurement of Soil Electrical Conductivity

Electrical conductivity is the capability of an element to transfer an electric current. It can be measured by calculating a change in electric current passing through electrodes on both sides of an element. From the electrical change rate, it is feasible to deduce the conductivity of soil of a specific area of the field as a representative property of soil of that particular area via soil electrical resistivity using the second Ohm's law [74].

Electrical resistivity can be expressed according to Ohm's law as:

$$R = \frac{\Delta V}{I} \tag{2}$$

where R is electrical resistance (Ω), ΔV is the voltage difference (V), and I is the electrical current (A).

For a homogeneous conductor, resistance is related to electrical resistivity ρ by:

$$R = \rho \frac{L}{A} \tag{3}$$

where L is the conductor length (m) and A is the cross-sectional area (m^2). Electrical conductivity σ is defined as the inverse of resistivity:

$$\sigma = \frac{1}{\rho}. \tag{4}$$

Equations (2)–(4) summarize the theoretical relationships between electrical resistance, resistivity, and electrical conductivity. In practice, the handheld EC sensor used in this study internally applies these relationships to convert measured voltage and current into an apparent soil electrical conductivity value, without requiring explicit calculation of L or A by the operator [75–77].

EC is usually denoted in units of milliSiemens per meter ($mS\,m^{-1}$) or deciSiemens per meter ($dS\,m^{-1}$), where 1 $dS\,m^{-1}$ = 100 $mS\,m^{-1}$ [78]. In this study, a handheld EC sensor with two metal electrodes was used to measure the EC of the soil. A fixed voltage signal was sent across the electrodes, causing an electrical current to transmit through the soil. The EC probe consisted of two metal electrodes inserted vertically into the soil to the target measurement depth at each depth layer. Measurements were taken with firm soil–electrode contact ensured by manual insertion, and EC values were recorded after signal stabilization. At each depth layer and moisture treatment, three EC readings were collected and averaged. Between measurements, the probe electrodes were cleaned to ensure consistent soil–electrode contact and minimize contact resistance effects. All EC measurements were performed at ambient laboratory temperature; temperature effects were assumed negligible under controlled soil-bin conditions (Figure 2).

2.2.4. Measurement of Soil Penetration, Shear Resistance, and EC at Different Levels of Soil Moisture

Three levels of moisture content were considered in the study (13%, 18%, and 22%) on a dry basis (db.). A soil moisture content of 22% was taken as field capacity [79], while a moisture content of 13% was considered as tilling moisture [80]. To obtain the desired moisture content in the soil, a calculated amount of water was added to dry soil, and the soil was allowed to equilibrate prior to measurement. The targeted moisture levels were verified using a time-domain reflectometry (TDR) soil moisture meter as well as the dry-oven method [81]. Although target moisture contents were verified prior to measurement, small spatial and depth-wise variations in water content may have persisted during the

experimental period; such variability is treated as an experimental limitation given the sensitivity of soil strength and EC to moisture.

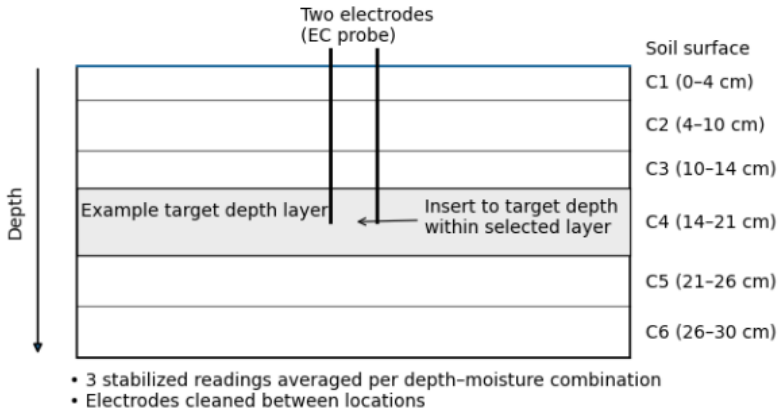

Figure 2. Schematic of EC probe installation for depth-layer measurements in the soil bin. Two electrodes were inserted vertically to the target depth within each depth layer (C1–C6), and three stabilized readings were averaged at each depth-layer–moisture combination.

Soil penetration resistance, shear resistance, and electrical conductivity were then measured across the identified depth layers (C1–C6) and at the three moisture levels using the aforementioned instruments, and expressed in MPa, kPa, and mS m^{-1}, respectively.

2.3. Identification of Depth Layers with Distinct Compaction States

Since the soil bin has been in use for the last 10 years for different soil tillage studies, depth-structured variability in soil strength was expected within the 0–30 cm profile. A continuous penetration-resistance profile was first measured with depth to identify breakpoints where soil mechanical resistance changed markedly. Based on this profile, six depth layers (C1–C6) were defined (Figure 3) that differed in penetration resistance (Table 1). These layers represent depth intervals with distinct inherent compaction states arising from long-term soil-bin conditioning, rather than independently imposed compaction treatments at each depth.

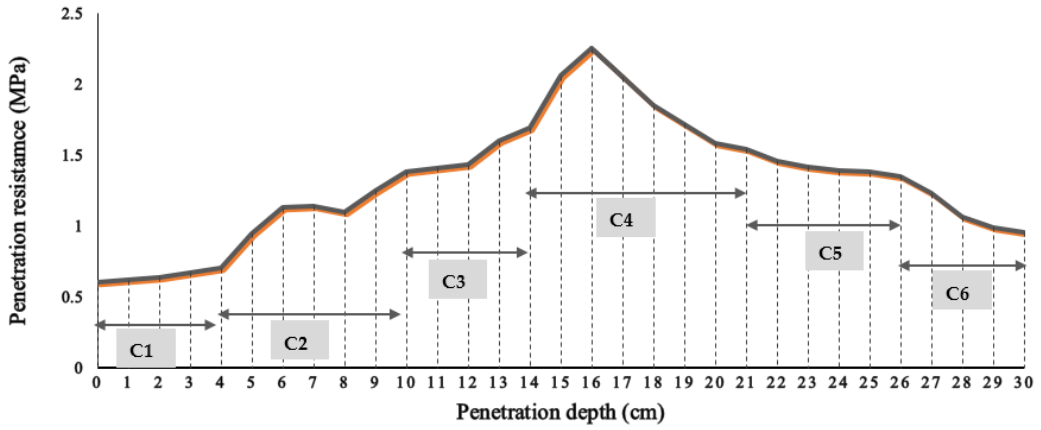

Figure 3. Identified depth layers with distinct compaction states. C1: 0–4 cm; C2: 4–10 cm; C3: 10–14 cm; C4: 14–21 cm; C5: 21–26 cm; C6: 26–30 cm.

Table 1. The average value of penetration resistance for each depth.

Penetration Depth (cm)	Penetration Resistance (MPa)
C1, 0–4	0.590
C2, 4–10	0.828
C3, 10–14	1.271
C4, 14–21	2.159
C5, 21–26	1.577
C6, 26–30	1.162

2.4. Preparation of the Soil Bin

Soil preparation was carried out based on the conditions required for the experiment. The soil bin was divided into three plots, each with different levels of moisture content. This preparation was achieved by adding water and using a carriage-mounted implement to condition and level the soil surface after moisture application [82]. No independent compaction treatments were imposed at specific depths. Instead, the soil bin exhibited depth-structured variability in soil strength resulting from long-term use in multiple tillage experiments. Accordingly, the defined depth layers (C1–C6) represent observational strata with distinct inherent compaction states identified from the penetration-resistance profile, rather than controlled traffic or loading treatments applied uniformly at each depth.

2.5. Experimental Design

The research was carried out in a soil bin under controlled conditions with three levels of soil moisture content (13, 18, and 22% db.) evaluated across six depth layers (C1–C6; 0–30 cm) characterized by distinct penetration-resistance profiles. Soil penetration resistance, shear resistance, and electrical conductivity (EC) were evaluated as response variables. Measurements were replicated three times for each depth-layer–moisture combination, providing replicate observations for statistical analysis. The parameters considered in the trial are summarized in Table 2.

Table 2. Factors and levels considered in the soil-bin experiment.

Factor	Levels
Soil moisture content (% db.)	13, 18, 22
Depth layer (cm)	C1: 0–4; C2: 4–10; C3: 10–14; C4: 14–21; C5: 21–26; C6: 26–30

Data were collected at 0–4, 4–10, 10–14, 14–21, 21–26, and 26–30 cm depths using a hand-pushed penetrometer and a soil shear resistance tester to specify the soil resistance to penetration and shear stress, respectively. Data were also collected for soil EC and moisture content at the same depth ranges using a soil moisture meter and a soil EC sensor.

To obtain a measurement of soil moisture content of soil, undisturbed soil samples were collected for the soil depths of 0–4, 4–10, 10–14, 14–21, 21–26, and 26–30 cm three times using sampling cores of 100 cm^3 volume and internal diameter of 5 cm. After being weighted, samples were kept in an oven (NUVE FN 120 oven, Nuve Sanayi Malzemeleri, Ankara, Turkey) for 24 h at 105 °C before instruments were applied to them. The values of moisture content for the soil samples were obtained by weighing the samples on a dry basis [83].

2.6. Field Validation Experiment

To evaluate the applicability of the laboratory-based models under practical conditions, a field validation experiment was conducted in a paddy field with sandy clay soil of similar

texture to that used in the soil bin. The experimental site and the root imaging system used for validation are illustrated in Figure 4.

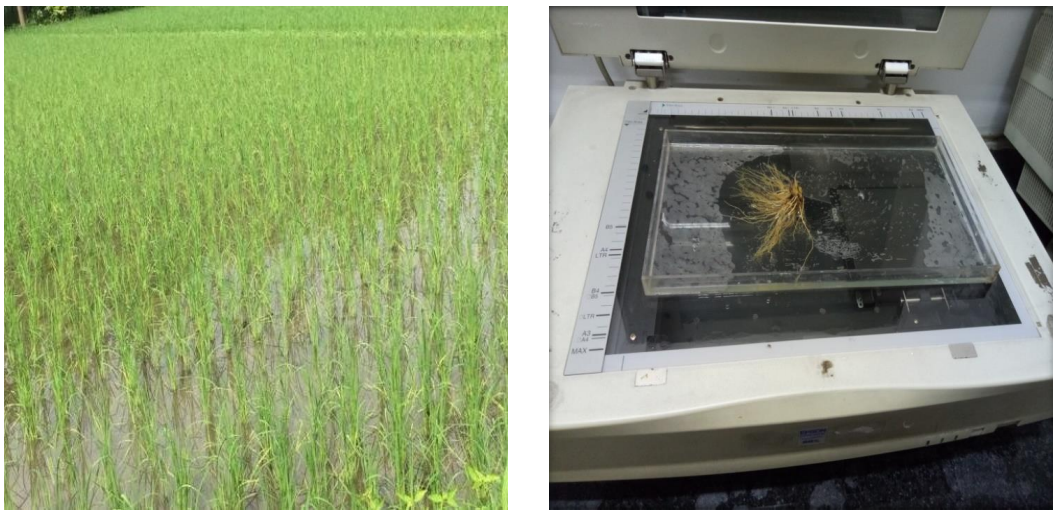

(a) (b)

Figure 4. Paddy crop under field conditions (**a**) and root growth analysis using WinRHIZO (**b**).

2.6.1. Root Sampling, Processing, and Analysis

Three levels of machine-induced compaction were created using a tractor-mounted rotary tiller operated at 540 PTO rpm, a rotor speed of 260 rpm, and a working width of 1.52 m. Tillage passes were applied 60 times (RT1: high compaction), 40 times (RT2: medium compaction), and 20 times (RT3: low compaction). Paddy seedlings (25 days old) were transplanted manually at a density of two to three seedlings per hill. Fertilization followed recommended practices, with applications of 150 kg N ha^{-1}, 60 kg P_2O_5 ha^{-1}, and 40 kg K_2O ha^{-1}. Half of the nitrogen and all phosphorus and potassium were applied after puddling, and the remaining nitrogen was top-dressed in two equal splits at 30 and 60 days after transplanting (DAT).

Root sampling was carried out at 60 DAT to assess vertical and horizontal root distribution under different compaction intensities. Soil cores were collected using a steel core sampler (internal diameter: 5 cm) at depth intervals of 0–15 cm, 15–30 cm, and 30–45 cm. For each plant, a central core was extracted at the plant base, and four additional cores were taken 2 cm to the left and right, representing three lateral zones: central (−2.5 to 2.5 cm), intermediate (4.5 to 9.5 cm), and outer (11.5 to 16.5 cm).

Excavated samples were processed using a modified wet-washing method based on [84]. Samples were soaked overnight in water containing a small amount of sodium hexametaphosphate to disperse soil aggregates. Floating roots were decanted through a fine mesh, and the washing and sieving procedure was repeated three times to ensure complete recovery. Cleaned root samples were gently air-dried until excess moisture was removed without causing clumping.

Root imaging and morphological measurements were performed using a WinRHIZO® Pro system (Regent Instruments Inc., Quebec, QC, Canada 2021). Roots were spread evenly in a thin layer of water on a transparent tray to minimize overlap during scanning. Imaging was conducted using the transparency unit (TPU), which provides top-down illumination for producing high-contrast silhouettes. WinRHIZO software was used to quantify total root length (RL), root surface area (RSA), average root diameter (RD), root volume (RV), and root length density (RLD). RLD was calculated as the total root length per unit volume of the sampled core.

For spatial visualization, RLD values were georeferenced according to their lateral and vertical sampling coordinates. Three-dimensional maps of RLD distribution were generated using the inverse distance weighted (IDW) interpolation method in ArcGIS Pro 2.8 enabling analysis of root system responses across the soil profile under varying compaction intensities.

Root sampling was performed on multiple plants within each compaction treatment (RT1–RT3). For each sampled plant, one central core and four additional lateral cores were collected at each of the three depth intervals (0–15, 15–30, and 30–45 cm). Thus, each plant contributed multiple soil cores spanning both vertical and lateral positions. The field root measurements are therefore interpreted as a qualitative consistency check rather than a statistically powered comparison among treatments.

2.6.2. Field Penetration Resistance Measurement

Soil penetration resistance in the field validation plots was measured using a hand-operated cone penetrometer following the same insertion approach as used in the soil-bin experiment. Measurements were taken within the depth range corresponding to the most resistant layer identified in the soil-bin profile (14–21 cm). For each compaction treatment (RT1–RT3), penetration resistance was measured at multiple locations within the plot, and mean penetration resistance values were used for comparison with model predictions.

2.7. Model Interpretability and Sensitivity Analysis

To interpret the influence of the data features on the prediction performance of the model and to quantify their impact on the outputs, two complementary methods were used: SHAP (SHapely Additive exPlanations) and Sobol sensitivity analysis.

SHAP is a unified framework for interpreting machine learning models based on cooperative game theory. It attributes to each feature an importance value, known as a SHAP value which represents the marginal contribution of that feature to the prediction and averaged over all possible feature combinations. SHAP values are additive and locally accurate, allowing for both global and instance-level interpretation of the relationship between the features with respect to the model outputs.

Sobol sensitivity analysis is a variance-based global sensitivity analysis method that decomposes the output variance of a model into contributions from each input feature and their interactions. The first-order Sobol index (S1) represents the proportion of output variance of a single feature acting alone. The higher-order indices capture interactive effects. This method provides a robust quantification of how each input impacts output variability, independent of the specific dataset used to train the model.

2.8. Statistical Analysis

Data from the soil-bin experiment were analyzed using analysis of variance (ANOVA) to evaluate the effects of depth layer and soil moisture content on penetration resistance, shear resistance, and electrical conductivity. Depth layers (C1–C6) correspond to predefined soil depth intervals with distinct inherent compaction states identified from the penetration resistance profile, rather than independently imposed compaction treatments.

Measurements were collected with three replications at each combination of depth layer and soil moisture content. For ANOVA, replicate measurements were averaged within each depth-layer–moisture combination, resulting in 18 treatment means (six depth layers $\times$ three moisture levels). This mean-based ANOVA was used to evaluate dominant main effects of depth layer and moisture content while reducing small-scale variability among replicate measurements.

Because averaging yields a single value per depth-layer–moisture combination, the depth layer $\times$ moisture interaction cannot be tested independently of residual error in

this mean-based ANOVA. Accordingly, ANOVA results are used here to establish primary depth and moisture effects prior to regression modeling. Potential interaction behavior is instead illustrated through regression response surfaces and discussed qualitatively.

Statistical significance was assessed at $p < 0.05$. Linear regression models relating penetration resistance and shear resistance to soil electrical conductivity and moisture content were subsequently fitted using ordinary least squares in Minitab 19.1 (Minitab LLC, State College, PA, USA).

3. Results

3.1. Results on Soil Penetration Resistance at Different Levels of Soil Moisture Content and Soil Depth Layers

Soil penetration resistance at different levels of soil moisture content and depth indicated that penetration resistance increased from the shallow layers to the most resistant depth layer (C4) and decreased again below that layer (Table 3). Soil resistance to penetration was found to be increased significantly at the highest depth layer of C4, at a depth of 14–21 cm, and specifically at the moisture level of 13% (ML1). The maximum soil penetration resistance was 2.422 MPa observed at a moisture content of 13%, which reduced to 1.932 MPa at 22% moisture content level for the same depth layer (C4). In general, increasing moisture content decreased penetration resistance, while penetration resistance increased from the shallow layers to C4 and decreased below C4 (Figure 5, Table 4).

Table 3. Soil penetration resistance (MPa) at different soil moisture contents and depth layers.

Depth Layer (Depth, cm)	ML1 (13%)	ML2 (18%)	ML3 (22%)
C1 (0–4)	0.693	0.582	0.494
C2 (4–10)	0.993	0.851	0.641
C3 (10–14)	1.433	1.270	1.110
C4 (14–21)	2.422	2.122	1.932
C5 (21–26)	1.835	1.513	1.383
C6 (26–30)	1.442	1.233	0.812

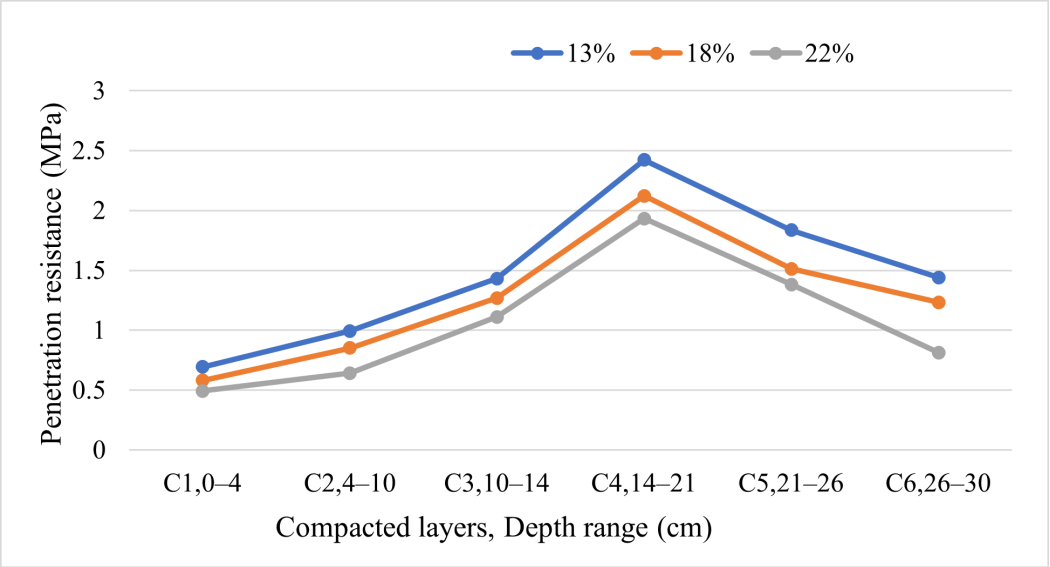

Figure 5. Soil penetration resistance at different moisture levels across the identified depth layers (C1–C6).

Table 4. Analysis of variance for the effects of soil depth layers and moisture content on soil penetration resistance.

Factor	DF	*p*-Value
Depth layer	5	0.000
Moisture content	2	0.000
Error	10	—
Total	17	—

These ANOVA results are based on treatment means and are intended to confirm dominant depth-layer and moisture effects prior to regression modeling rather than to provide a full factorial interaction analysis.

3.2. Results on Soil Shear Resistance at Different Soil Moisture Levels Across Depth Layers

The minimum soil shear resistance was observed in the shallowest depth layer (C1), which differed from the deeper layers (Table 5). The maximum shear resistance was observed in the most resistant depth layer (C4) across all moisture levels. The maximum (46.33 kPa) and minimum (26.33 kPa) shear resistance were observed for depth layer C4 at 13% moisture and for depth layer C1 at 22% moisture, respectively. Overall, shear resistance increased toward the most resistant depth layer and decreased with increasing soil moisture content (Figure 6, Table 6).

Table 5. Soil shear resistance (kPa) at different soil moisture contents and soil depth layers.

Depth Layer (Depth, cm)	ML1 (13%)	ML2 (18%)	ML3 (22%)
C1 (0–4)	31.33	28.33	26.33
C2 (4–10)	32.67	33.67	29.93
C3 (10–14)	41.33	37.67	32.67
C4 (14–21)	46.33	43.67	39.67
C5 (21–26)	35.67	33.00	30.33
C6 (26–30)	30.67	29.33	27.33

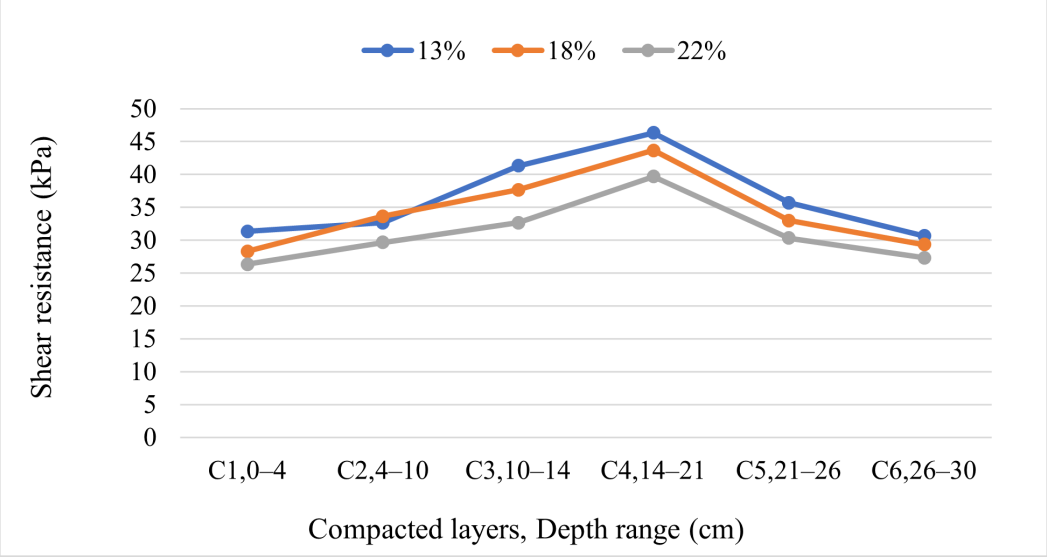

Figure 6. Soil shear resistance at different moisture content and different depth layers.

Table 6. Analysis of variance for the effects of soil depth layers and moisture content on soil shear resistance.

Source	DF	*p*-Value
Depth layer	5	0.000
Moisture content	2	0.000
Error	10	—
Total	17	—

3.3. Results on Soil Electrical Conductivity at Different Soil Moisture and Depth Layers

Soil electrical conductivity (EC) increased significantly with higher soil moisture content and toward the most resistant depth layer (Table 7). EC rose from 0.57 mS m^{-1} under the lowest moisture level (13%) and shallowest depth layer (C1, 0–4 cm) to 1.23 mS m^{-1} at the highest moisture level (22%) and the most resistant depth layer (C4, 14–21 cm).

Table 7. Soil electrical conductivity (mS m^{-1}) at different soil moisture contents and soil depth layers.

Depth Layer (Depth, cm)	ML1 (13%)	ML2 (18%)	ML3 (22%)
C1 (0–4)	0.57	0.63	0.72
C2 (4–10)	0.63	0.69	0.79
C3 (10–14)	0.79	0.90	1.01
C4 (14–21)	0.93	1.05	1.23
C5 (21–26)	0.76	0.83	0.98
C6 (26–30)	0.72	0.79	0.88

Among all treatments, the 14-21 cm depth consistently exhibited the highest EC values, indicating that EC increased toward the most resistant depth layer regardless of moisture content. These trends were clearly reflected in both the EC distribution patterns (Figure 7) and the corresponding ANOVA results (Table 8).

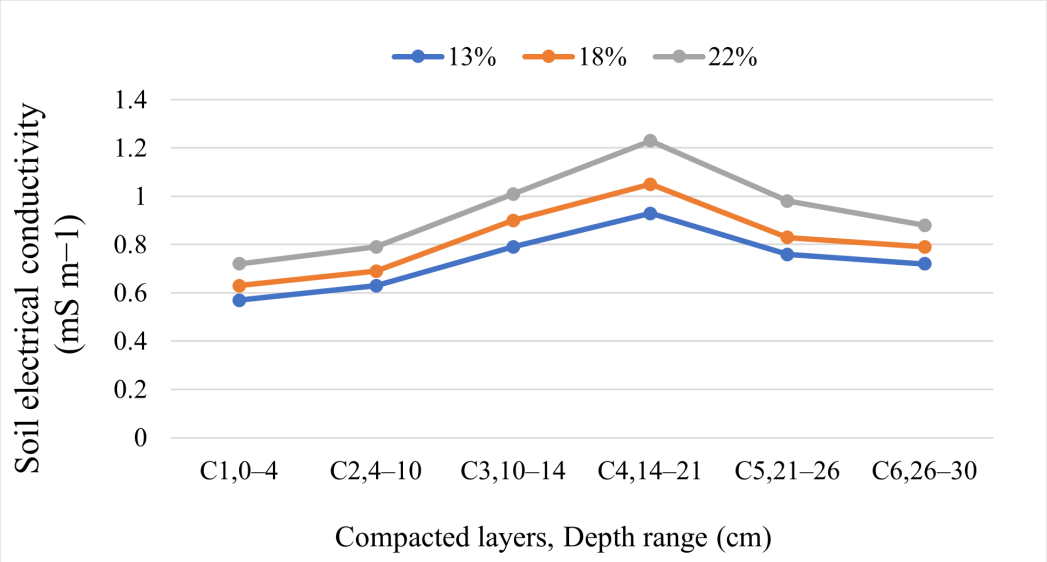

Figure 7. Soil electrical conductivity at different moisture levels across the identified depth layers (C1–C6).

Table 8. Analysis of variance for the effects of soil depth layer and moisture content on soil electrical conductivity.

Source	DF	*p*-Value
Depth layer	5	0.000
Moisture content	2	0.000
Error	10	—
Total	17	—

3.4. Regression Models for Depth-Resolved Soil Strength Estimation

Based on these relationships, linear regression models were developed to estimate penetration resistance and shear resistance from soil electrical conductivity (EC) and moisture content across the identified depth layers. Surface plots illustrating the fitted relationships are shown in Figures 8 and 9. These models provide a calibration basis for future sensing approaches that combine EC and moisture measurements to support depth-specific assessment of soil mechanical resistance.

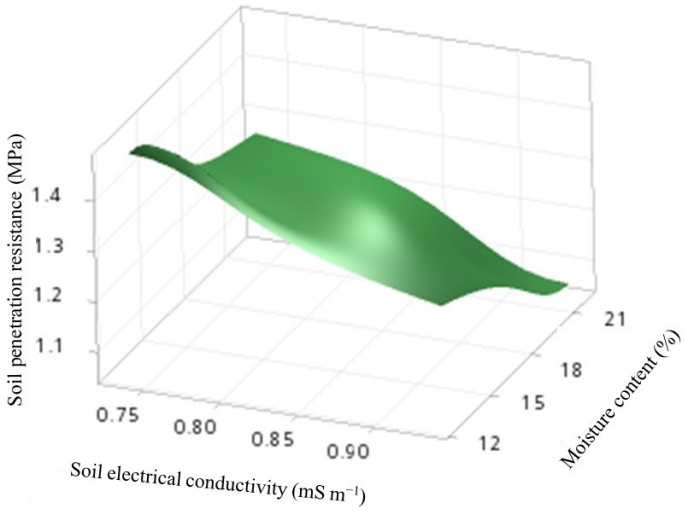

Figure 8. Surface plot of correlation of penetration resistance, moisture content, and soil electrical conductivity.

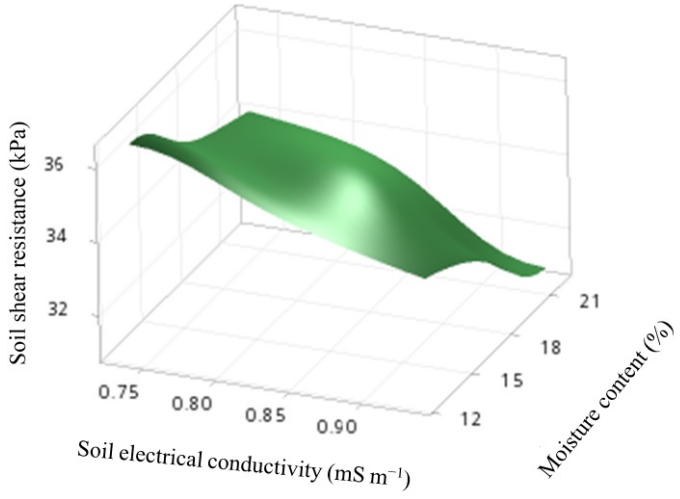

Figure 9. Surface plot showing the relationship among soil shear resistance, soil moisture content, and soil electrical conductivity.

A significant correlation was observed between soil electrical conductivity (EC) and soil moisture content across all depth layers, as well as between EC and soil shear strength. The regression models developed from these relationships are presented below.

(i) Soil penetration resistance

$$Pr = -0.1202\,x + 3.385\,y + 0.585 \quad (5)$$

The fitted model achieved $R^2 = 0.893$.

Where Pr is soil penetration resistance (MPa); x is soil moisture content (%); y is soil electrical conductivity (mS m^{-1}); and R^2 is the coefficient of determination.

(ii) Soil shear resistance

$$\tau_f = -1.265\,x + 30.91\,y + 30.66 \quad (6)$$

The fitted model achieved $R^2 = 0.782$.

Where τ_f is soil shear resistance (kPa); x is soil moisture content (%); y is soil electrical conductivity (mS m^{-1}); and R^2 is the coefficient of determination.

Equations (5) and (6) describe the linear relationships used to estimate penetration resistance and shear resistance from soil electrical conductivity and moisture content.

The linear regression models were fitted using treatment means ($n = 18$; six depth layers × three moisture levels). Visual inspection of residuals did not indicate strong departures from linearity within the tested ranges of EC and moisture content. Because soil electrical conductivity and moisture content are physically coupled, their correlation is acknowledged, and regression coefficients should be interpreted as empirical and conditional within the tested soil type and experimental conditions rather than as independent causal effects.

The data showed that when depth layer (reflecting depth-structured compaction state) and moisture were considered alongside EC in the model, EC and moisture together provided a useful empirical basis for estimating depth-resolved soil mechanical resistance within the tested soil-bin profile. However, there is a need to further study this relationship in different soil types, and taking into consideration the potential interference of factors such as salinity, pH, soil N, soil texture, organic matter, and soil cation exchange capacity (CEC).

Validation Results of Developed Prediction Models

The results revealed that the difference between model-predicted and measured penetration resistance values ranged from 3–6% under the specific field conditions tested, indicating close agreement under the specific field conditions and the limited number of compaction treatments evaluated (three levels). In addition, soil compaction effects were clearly reflected in root growth parameters (Table 9).

The mean root volume followed the order RT3 (9.41×10^3 cm^3) > RT2 (8.4×10^3 cm^3) > RT1 (7.8×10^3 cm^3), indicating progressively greater root development with decreasing compaction intensity. Maximum root-axis elongation (derived from WinRHIZO root length measurements) showed a similar trend, with RT3 (41.58 cm) > RT2 (31.85 cm) > RT1 (27.42 cm).

In the spatial distribution of root characteristics, root length density (RLD) was highest for RT3 (0.206 cm cm^{-3}), followed by RT2 (0.20 cm cm^{-3}) and RT1 (0.189 cm cm^{-3}). Similarly, root volume density (RVD) followed the trend RT3 (10.27 cm^3 cm^{-3}) > RT2 (9.18 cm^3 cm^{-3}) > RT1 (6.95 cm^3 cm^{-3}), confirming that higher compaction restricted root system development.

Table 9. Field validation results: penetration resistance prediction accuracy and associated root growth parameters.

Compaction Level	EC (mS m^{-1})	Moisture (%)	Penetration Resistance (MPa)			Root Growth		
			Model Predicted	Actual	Abs. Error (%)	Mean Root Volume (cm^3)	Root Elongation (cm)	Root Length Density (cm cm^{-3})
RT1 (60 passes)	1.13	14.6	2.65513	2.76	3.95	7.8×10^3	27.42	0.189
RT2 (40 passes)	1.04	16.7	2.09806	2.01	4.20	8.4×10^3	31.85	0.200
RT3 (20 passes)	0.91	15.3	1.82629	1.93	5.68	9.41×10^3	41.58	0.206

3.5. Machine-Learning-Based Prediction and Interpretability

Due to the relatively small dataset and the controlled nature of the experimental conditions, extended analysis was conducted to ensure that the prediction models captured meaningful, physically consistent relationships rather than artifacts of overfitting. To achieve this, feature interaction engineering, ensemble modeling, and post hoc interpretability techniques were applied.

For this analysis, a total of $N = 54$ observations from the soil-bin experiment (6 depth layers $\times$ 3 moisture levels $\times$ 3 replications) were used to train and evaluate the machine-learning models (Table 10). Although the dataset is relatively small, it represents the complete factorial combination of depth layers, moisture levels, and experimental replications under controlled conditions. A gradient boosting model was developed to predict soil penetration resistance from soil moisture content, electrical conductivity (EC), shear resistance (τ_f), and their interaction (EC $\times$ moisture). The model achieved a test score of $R^2 = 0.50$ with an RMSE of 0.43 MPa, indicating moderate predictive accuracy. Group-aware cross-validation using GroupKFold, with groups defined by depth-layer–moisture combinations, yielded R^2 values ranging from 0.10–0.66 (mean $\mu \approx 0.45$), reflecting variation in generalization across groups but consistently explaining a substantial portion of the variance.

Table 10. GroupKFold cross-validation R^2 scores by depth-layer–moisture groups.

Fold	R^2 Score
1	0.6647
2	0.1003
3	0.5870
Mean (μ)	**0.4507**

To assess whether the model learned physically meaningful signals, SHAP (Shapley Additive exPlanations) was used to quantify each feature's contribution to predictions. The SHAP summary plot (Figure 10) demonstrated that shear resistance (τ_f) was the dominant predictor of penetration resistance. EC and moisture content provided moderate but consistent contributions whose directions aligned with soil mechanics expectations: higher EC and lower moisture tended to increase penetration resistance. The EC $\times$ moisture interaction term captured subtle nonlinear effects but contributed less overall. Importantly, this ranking of feature importance (shear $>$ EC $\approx$ moisture $>$ interaction) closely matched the trends observed in the linear regression models, reinforcing internal consistency across modeling approaches.

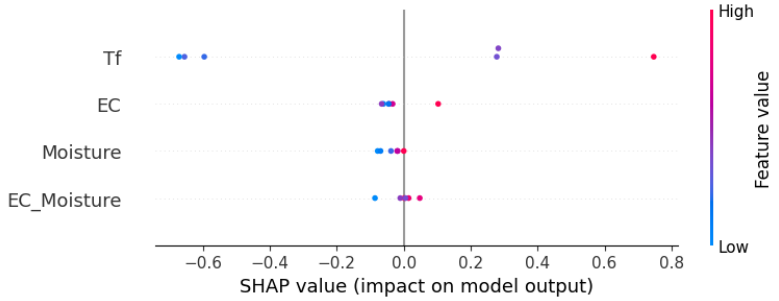

Figure 10. SHAP summary plot showing feature impact on the model output. Shear resistance (τ_f) has the strongest influence on predicted penetration resistance, followed by EC and moisture content.

Complementary global sensitivity analysis using Sobol first-order indices (S_1) further validated these findings (Table 11). Shear resistance exhibited a dominant first-order sensitivity index ($S_1 = 0.969$), confirming its role as the primary driver of variance in predicted penetration resistance. Because shear resistance is itself a direct mechanical measurement closely related to penetration resistance, its dominance in the feature rankings should not be interpreted as evidence that EC and moisture alone can replace mechanical sensing, but rather as a consistency check that the model aligns with established soil mechanics. EC, moisture, and their interaction demonstrated smaller but non-zero contributions ($S_1 < 0.02$), consistent with their supportive but secondary roles in influencing soil mechanical behavior.

Table 11. First-order Sobol sensitivity indices (S_1) for model input features.

Feature	Sobol S_1 Index
Moisture	0.001
EC	0.015
Shear resistance (τ_f)	0.969
EC × Moisture	0.008

Additionally, ordinary least squares (OLS) confidence interval analysis showed wider parameter uncertainty due to the limited dataset, justifying the use of ensemble techniques for more stable performance.

Taken together, the SHAP interpretability, Sobol sensitivity indices, and consistent alignment with physical soil behavior demonstrate that, even under data-limited conditions, the model learned meaningful and coherent relationships among soil moisture, EC, shear resistance, and penetration resistance. These findings support the feasibility of using EC and moisture content—after appropriate calibration—to support future real-time identification (after soil-specific calibration) of compacted soil layers, and highlight the potential of integrating interpretable machine learning into site-specific tillage and soil sensing systems.

It is important to note that the linear EC–moisture models constitute the primary operational prediction tools due to their simplicity and high R^2 under controlled conditions, whereas the gradient boosting model and associated SHAP/Sobol analyses were used in an exploratory fashion to assess feature importance and robustness under data-limited conditions.

4. Discussion

This study quantified how soil electrical conductivity and moisture content relate to penetration resistance and shear strength across the identified depth layers in a sandy clay soil, and evaluated whether these relationships can be exploited to support future real-time identification (after soil-specific calibration) of compacted layers. Overall, the results showed consistent and physically interpretable trends: increasing compaction increased

soil strength and EC, while increasing moisture content reduced penetration and shear resistance and generally increased EC. The regression models linking penetration resistance and shear resistance to EC and moisture achieved coefficients of determination (R^2) of 0.893 and 0.782, respectively, and showed 3–6% deviation between predicted and measured penetration resistance in the limited field validation. These findings suggest that EC and moisture, taken together, can serve as practical proxies for locating compacted layers.

4.1. Soil Moisture, Compaction, and Mechanical Resistance

Penetration resistance increased with depth layer and decreased with increasing moisture content across all layers, with the highest values observed in the most resistant depth layer (C4, 14–21 cm) at the lowest moisture level (13%). This pattern is consistent with previous observations in sandy loam, sandy clay loam, and clay loam soils, where higher water contents reduce mechanical impedance by lubricating particle contacts and lowering effective stress, whereas compaction increases bulk density and decreases pore connectivity, amplifying resistance to root and tool penetration [58,85–87]. Similar trends were observed for shear resistance, with maximum values again occurring in layer C4 at low moisture and minimum values in the shallow, least compacted layer at high moisture.

Mechanistically, these results reflect the interplay between soil water and the soil skeleton. At lower water contents, capillary forces and interparticle bonds increase, raising the apparent cohesion and internal friction angle and resulting in higher shear strength [72,88–91]. At higher water contents, these forces diminish and soil strength declines. The compaction-induced increase in bulk density further elevates both penetration and shear resistance by reducing pore volume and increasing the number of contacts per particle. The observed sensitivity of penetration resistance and shear strength to moisture and compaction in this study therefore aligns with established soil mechanics and root growth literature [13,14,16,21,92,93].

4.2. Electrical Conductivity as a Proxy for Compacted Layers

Soil EC in this study ranged from 0.57 to 1.23 mS m^{-1} across the tested combinations of moisture and depth layers. EC increased with compaction and, for a given depth layer, generally increased with moisture content. These trends are coherent with the dual dependence of EC on water-filled porosity and ion mobility. As moisture content rises, more of the pore space becomes water-filled, enhancing the continuity of conductive pathways and increasing EC [94–97]. Compaction, meanwhile, reduces macroporosity but can increase the area of water-filled contact between particles, which may also raise EC if salinity and ionic composition remain similar [61,62,98].

The observed relationships between EC, moisture, and compaction agree with prior studies that have reported significant correlations between EC (or electrical resistivity) and soil water content, bulk density, and penetration resistance [54,58–60,63,99–104]. This study extends that work by explicitly linking EC and moisture to both penetration resistance and shear strength through predictive models. Importantly, EC alone is not sufficient to diagnose compaction, as it is also influenced by salinity, clay content, organic matter, and temperature [52,105]. The combined use of EC and moisture content, as demonstrated here, provides a more robust basis for estimating the mechanical status of the soil.

4.3. Implications for Real-Time Sensing and Variable-Depth Tillage

The linear models developed in this study relate penetration resistance and shear resistance to EC and moisture content with relatively high R^2 values under controlled conditions. The field validation, which showed 3–6% deviation between predicted and measured penetration resistance (under the specific field conditions tested), suggests that the approach can be used to approximate the position of compacted layers in practice.

When integrated into an on-the-go sensing system, EC and moisture measurements could, in principle, be used to infer the depth and intensity of hardpan layers and drive real-time adjustment of tillage depth when implemented in an on-the-go system combining EC and TDR moisture sensors mounted near a tillage shank. Such a system would likely require co-located EC electrodes and a TDR moisture probe integrated near a shank or opener, enabling simultaneous measurement of EC and water content during tillage. This would allow farmers to avoid unnecessary deep tillage where the hardpan is shallow, reducing fuel use and protecting subsoil structure, while ensuring adequate fracture where compaction is severe [38,39,41,42].

The root system measurements in the field trial support the agronomic relevance of the modeled compaction patterns. Higher machine-induced compaction intensity (RT1 and RT2) was associated with reduced root length density and root development metrics, whereas the lower-compaction treatment (RT3) allowed larger and more extensive root systems. These trends are consistent with previous reports that compaction restricts root growth, alters root architecture, and reduces root access to deeper water and nutrients [27,28,106–109]. Thus, the ability to diagnose and selectively ameliorate compacted layers has direct implications for improving root functioning, crop resilience to drought, and yield stability [110–112].

Beyond the linear regression models, a gradient boosting model was explored to evaluate whether more flexible, data-driven methods could recover the same underlying relationships and to test the robustness of the feature correlations on a small dataset. Although the overall predictive performance of this model was moderate ($R^2 \approx 0.50$ on the test set, with GroupKFold R^2 scores ranging from 0.10 to 0.66), the interpretability analyses are informative. SHAP values consistently identified shear resistance as the dominant driver of predicted penetration resistance, with EC and moisture providing secondary contributions whose directions and magnitudes agreed with both the physical understanding of compaction and the coefficients of the linear models. Sobol sensitivity analysis likewise yielded a very high first-order sensitivity index for shear resistance and much smaller, but non-zero, indices for EC, moisture, and their interaction.

The key point is not that the ensemble model provides substantially better numerical accuracy than the simpler regressions, but that, even under data-limited conditions, it converges to a feature importance structure that is physically plausible and statistically coherent. This convergence serves as an internal consistency check: the model is learning a genuine signal rather than spurious patterns. In practical terms, the combination of (i) high R^2 values for the linear models under controlled conditions, (ii) low prediction error in the field validation, and (iii) agreement between the ML feature importance rankings and soil mechanics expectations, all reinforce the conclusion that EC and moisture content carry meaningful information about compaction state and can be used, after appropriate calibration, to support real-time identification of compacted layers.

4.4. Limitations and Future Work

This study was conducted on a single soil type (sandy clay: 48.6% sand, 29.3% clay, and 22.1% silt) under controlled soil-bin conditions, with field validation on a site of similar texture. While this approach allowed precise control over compaction and moisture, it also limited the immediate generalization of the models. Soil EC is known to be influenced by salinity, clay mineralogy, organic matter, cation exchange capacity, and temperature, among other factors [37,52,105]. The relationships observed here are therefore expected to hold qualitatively in soils of similar texture and chemical status, but quantitative model coefficients will likely differ in other soils.

Bulk density, soil pH, nutrient status, and aboveground biomass were not measured in the present study. While root system characteristics provide a direct indicator of compaction effects on plant development, future work should integrate these additional soil and crop variables to strengthen links between mechanical diagnostics, nutrient availability, and whole-plant performance.

Additional limitations include the relatively small number of moisture levels tested and the restricted range of EC values. The sample size for advanced machine learning analyses was also limited, which constrains the robustness of the SHAP and Sobol results. Future research should extend this work to multiple soil types (e.g., sandy loam, sandy clay loam, clay loam) and to field conditions experiencing dynamic climatic and management influences. Larger datasets, spanning broader gradients of moisture, salinity, and compaction, would enable more robust nonlinear modeling and evaluation of sensor performance. Furthermore, integrating EC and moisture sensing with on-the-go mechanical sensing (e.g., instrumented shanks) could produce hybrid systems that exploit both direct and indirect indicators of compaction, improving reliability for variable-depth tillage control.

Finally, prototype sensors and control algorithms should be tested in commercial fields over multiple seasons to quantify fuel savings, yield impacts, and long-term effects on soil structure. Such studies would close the loop from controlled experiments and modeling to operational precision tillage systems.

5. Conclusions

This study investigated the relationships among soil electrical conductivity, moisture content, penetration resistance, and shear strength in a sandy clay soil with multiple compacted layers, and evaluated the potential of EC and moisture measurements for supporting real-time identification of compacted layers. The main conclusions are:

1. Soil penetration resistance and shear strength increased with depth layer and decreased with increasing moisture content. The most resistant depth layer (C4, 14–21 cm) exhibited the highest penetration resistance (up to 2.42 MPa) and shear strength (up to 46.33 kPa), particularly at the lowest moisture level (13%). These trends are consistent with established soil mechanics and root growth responses to compaction and water availability.
2. Soil electrical conductivity ranged from 0.57 to 1.23 mS m^{-1} across the tested treatments and increased with both depth layer and moisture content. The combined behavior of EC and moisture reflects changes in water-filled pore space and conductive pathways associated with compaction and drying.
3. Linear regression models relating penetration resistance and shear resistance to EC and moisture content achieved coefficients of determination of 0.893 and 0.782, respectively. Field validation showed that model-predicted penetration resistance differed from measured values by 3–6% across the three compaction treatments evaluated, indicating that EC and moisture, taken together, showed preliminary agreement in approximating the mechanical status of compacted layers under the specific conditions tested in soils of similar texture.
4. Root system measurements in the field confirmed that higher compaction reduced root volume, root length density, and maximum rooting depth, while lower compaction allowed deeper and more extensive root growth. These results link the modeled compaction patterns directly to root functioning and potential crop performance.
5. Exploratory machine learning and sensitivity analyses indicated that shear resistance is the dominant predictor of penetration resistance, while EC and moisture contribute through interaction effects. This supports the use of EC and moisture as

indirect indicators that should be calibrated against mechanical measurements for specific soils.

Taken together, these findings demonstrate that soil electrical conductivity and moisture content can be used to identify compacted layers and estimate soil mechanical resistance with sufficient accuracy to support variable-depth tillage decisions. Implemented in an on-the-go sensing system, the proposed approach could reduce unnecessary deep tillage, improve fuel and energy-use efficiency, and help maintain soil structure and root-friendly conditions. Future work should extend model calibration and validation to a wider range of soil types and field environments, and integrate EC and moisture sensing with real-time control of tillage implements in commercial cropping systems.

Author Contributions: H.M.: Conceptualization, Methodology, Investigation, Formal analysis, Data curation, Writing—original draft; A.C.: Conceptualization, Methodology, Supervision, Validation, Resources, Writing—review & editing; R.P.: Data curation, Validation, Formal analysis, Writing—review & editing; A.M.H.: Formal analysis, Model validation, Writing—review & editing. All authors have read and agreed to the published version of the manuscript.

Funding: This research received no external funding.

Institutional Review Board Statement: Not applicable.

Data Availability Statement: The data presented in this study are available within the article.

Acknowledgments: The authors acknowledge the assistance received from Turkey Scholarship under The Republic of Turkey, Department of Agricultural Machinery and Technologies Engineering, Faculty of Agriculture, Ataturk University, Erzurum, during the study.

Conflicts of Interest: The authors declare no conflicts of interest.

References

1. Bajželj, B.; Richards, K.S.; Allwood, J.M.; Smith, P.; Dennis, J.S.; Curmi, E.; Gilligan, C.A. Importance of food-demand management for climate mitigation. *Nat. Clim. Change* **2014**, *4*, 924–929. [CrossRef]
2. Jat, M.L.; Chakraborty, D.; Ladha, J.K.; Rana, D.S.; Gathala, M.K.; McDonald, A.; Gerard, B. Conservation agriculture for sustainable intensification in South Asia. *Nat. Sustain.* **2020**, *3*, 336–343. [CrossRef]
3. Parray, R.A.; Mani, I.; Kumar, A.; Khura, T.K.; Lande, S.D. Pilot study of farm power-machinery status and custom-hiring opportunities in rice (*Oryza sativa*)–wheat (*Triticum aestivum*) cropping system. *Indian J. Agric. Sci.* **2016**, *86*, 167–172. [CrossRef]
4. Pedrera-Parrilla, A.; Brevik, E.C.; Giráldez, J.V.; Vanderlinden, K. Temporal stability of electrical conductivity in a sandy soil. *Int. Agrophysics* **2016**, *30*, 313–322. [CrossRef]
5. Pathak, H.S.; Brown, P.; Best, T. A systematic literature review of the factors affecting the precision agriculture adoption process. *Precis. Agric.* **2019**, *20*, 1292–1316. [CrossRef]
6. Shafi, U.; Mumtaz, R.; García-Nieto, J.; Hassan, S.A.; Zaidi, S.A.R.; Iqbal, N. Precision agriculture techniques and practices: From considerations to applications. *Sensors* **2019**, *19*, 3796. [CrossRef]
7. Soil Science Society of America. *Glossary of Soil Science Terms*; SSSA: Madison, WI, USA, 1996.
8. Orzech, K.; Wanic, M.; Załuski, D. The effects of soil compaction and different tillage systems on the bulk density and moisture content of soil and the yields of winter oilseed rape and cereals. *Agriculture* **2021**, *11*, 666. [CrossRef]
9. Colombi, T.; Braun, S.; Keller, T.; Walter, A. Artificial macropores attract crop roots and enhance plant productivity on compacted soils. *Sci. Total Environ.* **2017**, *574*, 1283–1293. [CrossRef]
10. Kim, H.; Anderson, S.H.; Motavalli, P.P.; Gantzer, C.J. Compaction effects on soil macropore geometry and related parameters for an arable field. *Geoderma* **2010**, *160*, 244–251. [CrossRef]
11. Hamza, M.A.; Anderson, W.K. Soil compaction in cropping systems: A review of the nature, causes and possible solutions. *Soil Tillage Res.* **2005**, *82*, 121–145. [CrossRef]
12. Richard, G.; Cousin, I.; Sillon, J.F.; Bruand, A.; Guérif, J. Effect of compaction on the porosity of a silty soil: Influence on unsaturated hydraulic properties. *Eur. J. Soil Sci.* **2001**, *52*, 49–58. [CrossRef]
13. Bengough, A.G.; Mullins, C.E. Mechanical impedance to root growth: A review of experimental techniques and root growth responses. *J. Soil Sci.* **1990**, *41*, 341–358. [CrossRef]

14. Bengough, A.G.; Mullins, C.E. Penetrometer resistance, root penetration resistance and root elongation rate in two sandy loam soils. *Plant Soil* **1991**, *131*, 59–66. [CrossRef]
15. Bengough, A.G.; Bransby, M.F.; Hans, J.; McKenna, S.J.; Roberts, T.J.; Valentine, T.A. Root responses to soil physical conditions; growth dynamics from field to cell. *J. Exp. Bot.* **2006**, *57*, 437–447. [CrossRef]
16. Bengough, A.G.; McKenzie, B.M.; Hallett, P.D.; Valentine, T.A. Root elongation, water stress, and mechanical impedance: A review of limiting stresses and beneficial root tip traits. *J. Exp. Bot.* **2011**, *62*, 59–68. [CrossRef]
17. Young, I.M.; Montagu, K.; Conroy, J.; Bengough, A.G. Mechanical impedance of root growth directly reduces leaf elongation rates of cereals. *New Phytol.* **1997**, *135*, 613–619. [CrossRef]
18. McKenzie, B.M.; Mullins, C.E.; Tisdall, J.M.; Bengough, A.G. Root–soil friction: Quantification provides evidence for measurable benefits for manipulation of root-tip traits. *Plant Cell Environ.* **2013**, *36*, 1085–1092. [CrossRef] [PubMed]
19. Jacobsen, A.G.; Jervis, G.; Xu, J.; Topping, J.F.; Lindsey, K. Root growth responses to mechanical impedance are regulated by a network of ROS, ethylene and auxin signalling in *Arabidopsis*. *New Phytol.* **2021**, *231*, 225–242. [CrossRef] [PubMed]
20. Håkansson, I.; Reeder, R.C. Subsoil compaction by vehicles with high axle load—Extent, persistence and crop response. *Soil Tillage Res.* **1994**, *29*, 277–304. [CrossRef]
21. Colombi, T.; Keller, T. Developing strategies to recover crop productivity after soil compaction—A plant eco-physiological perspective. *Soil Tillage Res.* **2019**, *191*, 156–161. [CrossRef]
22. de Moraes, M.T.; Debiasi, H.; Franchini, J.C.; Mastroberti, A.A.; Levien, R.; Leitner, D.; Schnepf, A. Soil compaction impacts soybean root growth in an Oxisol from subtropical Brazil. *Soil Tillage Res.* **2020**, *200*, 104611. [CrossRef]
23. Dörner, J.; Dec, D.; Peng, X.; Horn, R. Effect of land use change on the dynamic behaviour of structural properties of an Andisol in southern Chile under saturated and unsaturated hydraulic conditions. *Geoderma* **2010**, *159*, 189–197. [CrossRef]
24. Hillel, D. *Introduction to Environmental Soil Physics*; Elsevier Academic Press: San Diego, CA, USA, 2003.
25. Whalley, W.R.; Leeds-Harrison, P.B.; Clark, L.J.; Gowing, D.J.G. Use of effective stress to predict the penetrometer resistance of unsaturated agricultural soils. *Soil Tillage Res.* **2005**, *84*, 18–27. [CrossRef]
26. Daigh, A.L.M.; DeJong-Hughes, J.; Acharya, U. Projections of yield losses and economic costs following deep wheel-traffic compaction during the 2019 harvest. *Agric. Environ. Lett.* **2020**, *5*, e20013. [CrossRef]
27. Dong, W.C.; Fu, Q.; Wang, Q.J.; Cao, C.P. Effect of plough pans on the growth of soybean roots in the black-soil region of northeastern China. *J. Integr. Agric.* **2017**, *16*, 2191–2196. [CrossRef]
28. Lipiec, J.; Horn, R.; Pietrusiewicz, J.; Siczek, A. Effects of soil compaction on root elongation and anatomy of different cereal plant species. *Soil Tillage Res.* **2012**, *121*, 74–81. [CrossRef]
29. To, J.; Kay, B.D. Variation in penetrometer resistance with soil properties: The contribution of effective stress and implications for pedotransfer functions. *Geoderma* **2005**, *126*, 261–276. [CrossRef]
30. Mirreh, H.F.; Ketcheson, J.W. Influence of soil bulk density and matric pressure on soil resistance to penetration. *Can. J. Soil Sci.* **1972**, *52*, 477–483. [CrossRef]
31. Hernanz, J.L.; Peixoto, H.; Cerisola, C.; Sánchez-Girón, V. An empirical model to predict soil bulk density profiles in field conditions using penetration resistance, moisture content and soil depth. *J. Terramechanics* **2000**, *37*, 167–184. [CrossRef]
32. Busscher, W.J. Adjustment of flat-tipped penetrometer resistance data to a common water content. *Trans. ASAE* **1990**, *33*, 519–524. [CrossRef]
33. Ayers, P.D.; Perumpral, J.V. Moisture and density effect on cone index. *Trans. ASAE* **1982**, *25*, 1169–1172. [CrossRef]
34. Vaz, C.M.; Manieri, J.M.; de Maria, I.C.; Tuller, M. Modeling and correction of soil penetration resistance for varying soil water content. *Geoderma* **2011**, *166*, 92–101. [CrossRef]
35. Vaz, C.M.; Manieri, J.M.; de Maria, I.C.; van Genuchten, M.T. Scaling the dependency of soil penetration resistance on water content and bulk density of different soils. *Soil Sci. Soc. Am. J.* **2013**, *77*, 1488–1495. [CrossRef]
36. Zhang, W.; Gao, W.; Ren, T.; Whalley, W.R. A novel approach to estimate soil penetrometer resistance from water content, bulk density, and shear wave velocity: A laboratory study on a loamy sand soil. *Geoderma* **2020**, *368*, 114276. [CrossRef]
37. Huang, Y.; Jiang, H.; Wang, W.; Sun, D. Prediction model of soil electrical conductivity based on ELM optimized by Bald Eagle Search Algorithm. *Electronics* **2021**, *25*, 50–56. [CrossRef]
38. Raper, R.L.; Schwab, E.B.; Dabney, S.M.; Oxford, M.S. Spatial variation of the depth of the root restricting layer in an upland soil of northern Mississippi. In Proceedings of the Second International Conference on Geospatial Information in Agriculture and Forestry, Lake Buena, Vista, FL, USA, l0–12 January 2000; pp. 249–256.
39. Gorucu, S.; Khalilian, A.; Han, Y.J.; Dodd, R.B.; Smith, B.R. An algorithm to determine the optimum tillage depth from soil penetrometer data in Coastal Plain soils. *Appl. Eng. Agric.* **2006**, *22*, 625–631. [CrossRef]
40. Garner, T.H.; Musen, H.L.; Dodd, R.B. Management data for primary tillage of Coastal Plain soils. In Proceedings of the Beltwide Cotton Production Research Conferences, Las Vegas, NV, USA, 4–9 January 1986; pp. 465–466.
41. Fox, J.W.; Khalilian, A.; Han, Y.J.; Williams, P.B.; Nafchi, A.M.; Maja, J.M.; Marshall, M.W.; Barnes, E.M. Real-time, variable-depth tillage for managing soil compaction in cotton production. *Open J. Soil Sci.* **2018**, *8*, 147–161. [CrossRef]

42. Cortez, L.A.; Marques Junior, J.; Peluco, R.G.; Siqueira, D.S.; Siansi, F.L.; Barbosa, R.S.; Furlani, C.E.A.; Camargo, L.A.; Silva, L.S.; Gomes, R.P. Subsoiling of an Oxisol at fixed and varying depth in areas under sugarcane. *Precis. Agric.* **2020**, *21*, 1351–1365. [CrossRef]
43. Gorucu, S.; Khalilian, A.; Han, Y.J.; Dodd, R.B.; Wolak, F.J.; Keskin, M. Variable depth tillage based on geo-referenced soil compaction data in the Coastal Plain region of South Carolina. In Proceedings of the ASAE Annual Meeting, Sacramento, CA, USA, 30 July–1 August 2001; p. 1. [CrossRef]
44. Kichler, C.M.; Fulton, J.P.; Raper, R.L.; Zech, W.C.; McDonald, T.P.; Brodbeck, C.J. Spatially monitoring tractor performance to evaluate energy requirements of variable depth tillage and implement selection. In Proceedings of the ASAE Annual Meeting, Minneapolis, MN, USA, 17–20 June 2007; p. 1. [CrossRef]
45. Abbaspour-Gilandeh, Y.; Khalilian, A.; Reza, A.; Alireza, K.; Sadati, S.H. Energy savings with variable-depth tillage. In Proceedings of the 27th Southern Conservation Tillage Systems Conference, Florence, SC, USA, 27–29 June 2005; pp. 84–91.
46. Sabouri, Y.; Abbaspour-Gilandeh, Y.; Solhjou, A.; Shaker, M.; Szymanek, M.; Sprawka, M. Development and laboratory evaluation of an online controlling algorithm for precision tillage. *Sensors* **2021**, *21*, 5603. [CrossRef]
47. Schjønning, P. Topsoil shear strength—Measurements and predictions. *Soil Tillage Res.* **2021**, *212*, 105049. [CrossRef]
48. Stefanow, D.; Dudziński, P.A. Soil shear strength determination methods—State of the art. *Soil Tillage Res.* **2021**, *208*, 104881. [CrossRef]
49. Bailey, A.C.; Weber, J.A. Comparison of methods of measuring soil shear strength using artificial soils. *Trans. ASAE* **1965**, *8*, 153–156. [CrossRef]
50. Fleming, K.L.; Heermann, D.F.; Westfall, D.G. Evaluating soil color with farmer input and apparent soil electrical conductivity for management zone delineation. *Agron. J.* **2004**, *96*, 1581–1587. [CrossRef]
51. Jung, W.K.; Kitchen, N.R.; Sudduth, K.A.; Kremer, R.J.; Motavalli, P.P. Relationship of apparent soil electrical conductivity to claypan soil properties. *Soil Sci. Soc. Am. J.* **2005**, *69*, 883–892. [CrossRef]
52. Corwin, D.L.; Lesch, S.M. Characterizing soil spatial variability with apparent soil electrical conductivity: I. Survey protocols. *Comput. Electron. Agric.* **2005**, *46*, 103–133. [CrossRef]
53. Molin, J.P.; Castro, C.N.D. Establishing management zones using soil electrical conductivity and other soil properties by the fuzzy clustering technique. *Sci. Agric.* **2008**, *65*, 567–573. [CrossRef]
54. Valente, D.S.M.; Queiroz, D.M.; Pinto, F.A.C.; Santos, N.T.; Santos, F.L. The relationship between apparent soil electrical conductivity and soil properties. *Revista Ciência Agronômica* **2012**, *43*, 683–690. [CrossRef]
55. Martinez, G.; Vanderlinden, K.; Ordóñez, R.; Muriel, J.L. Can apparent electrical conductivity improve the spatial characterization of soil organic carbon? *Vadose Zone J.* **2009**, *8*, 586–593. [CrossRef]
56. Peralta, N.R.; Costa, J.L.; Balzarini, M.; Angelini, H. Delineation of management zones with measurements of soil apparent electrical conductivity in the southeastern Pampas. *Can. J. Soil Sci.* **2013**, *93*, 205–218. [CrossRef]
57. De Caires, S.A.; Wuddivira, M.N.; Bekele, I. Spatial analysis for management zone delineation in a humid tropic cocoa plantation. *Precis. Agric.* **2015**, *16*, 129–147. [CrossRef]
58. Bai, W.; Kong, L.; Guo, A. Effects of physical properties on electrical conductivity of compacted lateritic soil. *J. Rock Mech. Geotech. Eng.* **2013**, *5*, 406–411. [CrossRef]
59. Jeřábek, J.; Zumr, D.; Dostál, T. Identifying the plough pan position on cultivated soils by measurements of electrical resistivity and penetration resistance. *Soil Tillage Res.* **2017**, *174*, 231–240. [CrossRef]
60. de Melo, L.B.B.; Silva, B.M.; Peixoto, D.S.; Chiarini, T.P.A.; de Oliveira, G.C.; Curi, N. Effect of compaction on the relationship between electrical resistivity and soil water content in Oxisol. *Soil Tillage Res.* **2021**, *208*, 104876. [CrossRef]
61. Pentoś, K.; Pieczarka, K.; Serwata, K. The relationship between soil electrical parameters and compaction of sandy clay loam soil. *Agriculture* **2021**, *11*, 114. [CrossRef]
62. Kowalczyk, S.; Maślakowski, M.; Tucholka, P. Determination of the correlation between the electrical resistivity of non-cohesive soils and the degree of compaction. *J. Appl. Geophys.* **2014**, *110*, 43–50. [CrossRef]
63. Zhou, M.; Wang, J.; Cai, L.; Fan, Y.; Zheng, Z. Laboratory investigations on factors affecting soil electrical resistivity and the measurement. *IEEE Trans. Ind. Appl.* **2015**, *51*, 5358–5365. [CrossRef]
64. Dexter, A.R.; Czyż, E.A.; Gąte, O.P. A method for prediction of soil penetration resistance. *Soil Tillage Res.* **2007**, *93*, 412–419. [CrossRef]
65. Stelluti, M.; Maiorana, M.; De Giorgio, D. Multivariate approach to evaluate the penetrometer resistance in different tillage systems. *Soil Tillage Res.* **1998**, *46*, 145–151. [CrossRef]
66. *ASAE Standard S313.3*; Soil Cone Penetrometer. ASAE: St. Joseph, MI, USA, 2006.
67. Vaz, C.M.P.; de Resende, J.M.; Franchini, J.C.; Debiasi, H.; Nunes, M.R. Evaluation and recommendations for the use of dynamic penetrometers. *Soil Tillage Res.* **2022**, *220*, 105373. [CrossRef]
68. Medina, C.; Camacho-Tamayo, J.H.; Cortés, C.A. Soil penetration resistance analysis by multivariate and geostatistical methods. *Engenharia Agrícola* **2012**, *32*, 91–101. [CrossRef]

69. Naderi-Boldaji, M.; Alimardani, R.; Sharifi, A.; Tabatabaeefar, A. Economical hand-pushed digital cone penetrometer. *Int. Agrophysics* **2009**, *23*, 55–60.
70. Bradford, J.M. Penetrability. In *Methods of Soil Analysis: Part 1. Physical and Mineralogical Methods*; Soil Science Society of America: Madison, WI, USA, 1986; Volume 5, pp. 463–478.
71. American Society of Agricultural Engineers. *Agricultural Engineers Yearbook of Standards*; ASAE: St. Joseph, MI, USA, 1984; p. 819.
72. Mouazen, A.M.; Ramon, H.; De Baerdemaeker, J. Effects of bulk density and moisture content on selected mechanical properties of sandy loam soil. *Biosyst. Eng.* **2002**, *83*, 217–224. [CrossRef]
73. Nguyen, G.I.A.N.G. The analysis of factors influencing the values of soil shear strength parameters obtained by direct shear test. *Stud. Geotech. Et Mech.* **2009**, *31*, 51–72.
74. Telford, W.M.; Geldart, L.P.; Sheriff, R.E.; Keys, D.A. *Applied Geophysics*; Cambridge University Press: Cambridge, UK, 1990; Resistivity Methods, pp. 522–539.
75. Hassan, A.A.; Toll, D.G. Water content characteristics of mechanically compacted clay soil determined using the electrical resistivity method. In Proceedings of the XVI European Conference on Soil Mechanics and Geotechnical Engineering, Edinburgh, Scotland, 13–17 September 2015; pp. 3395–3400. [CrossRef]
76. Samouëlian, A.; Cousin, I.; Tabbagh, A.; Bruand, A.; Richard, G. Electrical resistivity survey in soil science: A review. *Soil Tillage Res.* **2005**, *83*, 173–193. [CrossRef]
77. Heaney, M.B. Electrical conductivity and resistivity. In *Electrical Measurement, Signal Processing, and Displays*; Webster, J.G., Ed.; CRC Press: Boca Raton, FL, USA, 2003.
78. Seifi, M.R.; Alimardani, R.; Sharifi, A. How can soil electrical conductivity measurements control soil pollution? *Res. J. Environ. Earth Sci.* **2010**, *2*, 235–238.
79. Cornell University. Soil and Water Management. PO 12.1–3. NRCCA Study Resources. 2021. Available online: https://nrcca.cals.cornell.edu/soil/CA2/CA0212.1-3.php (accessed on 27 September 2021).
80. Shittu, K.A.; Oyedele, D.J.; Babatunde, K.M. The effects of moisture content at tillage on soil strength in maize production. *Egypt. J. Basic Appl. Sci.* **2017**, *4*, 139–142. [CrossRef]
81. O'Kelly, B.C. Accurate determination of moisture content of organic soils using the oven drying method. *Dry. Technol.* **2004**, *22*, 1767–1776. [CrossRef]
82. Celik, A.; Raper, R.L. Design and evaluation of ground-driven rotary subsoilers. *Soil Tillage Res.* **2012**, *124*, 203–210. [CrossRef]
83. Malasli, M.Z.; Celik, A. Disc angle and tilt angle effects on forces acting on a single-disc type no-till seeder opener. *Soil Tillage Res.* **2019**, *194*, 104304. [CrossRef]
84. Aggarwal, P.; Choudhary, K.; Singh, A.; Chakraborty, D. Variation in soil strength and rooting characteristics of wheat in relation to soil management. *Geoderma* **2006**, *136*, 353–363. [CrossRef]
85. Thomas, P.; Mondal, S.; Roy, D.; Meena, M.; Aggarwal, B.; Sharma, A.; Behera, U.; Das, T.; Jatav, R.; Chakraborty, D. Exploring the relationships between penetration resistance, bulk density and water content in cultivated soils. *J. Agric. Phys.* **2020**, *20*, 22.
86. Moraes, M.T.D.; Debiasi, H.; Franchini, J.C.; Silva, V.R.D. Soil penetration resistance in a Rhodic Eutrudox affected by machinery traffic and soil water content. *Eng. Agrícola* **2013**, *33*, 748–757. [CrossRef]
87. Assis, R.L.D.; Lazarini, G.D.; Lanças, K.P.; Cargnelutti Filho, A. Avaliação da resistência do solo à penetração em diferentes solos com a variação do teor de água. *Eng. Agrícola* **2009**, *29*, 558–568. [CrossRef]
88. McKyes, E.; Nyamugafata, P.; Nyamapfene, K.W. Characterization of cohesion, friction and sensitivity of two hardsetting soils from Zimbabwe. *Soil Tillage Res.* **1994**, *29*, 357–366. [CrossRef]
89. Porter, M.A.; McMahon, T.A. MUTILLS—The Melbourne University tilled soil model. *Trans. ASAE* **1990**, *33*, 419–431. [CrossRef]
90. Kézdi, Á.; Rétháti, L. *Handbook of Soil Mechanics, Vol. 1: Soil Physics*; Elsevier: Amsterdam, The Netherlands, 1974.
91. Chancellor, W.J. Effects of compaction on soil strength. In *Compaction of Agricultural Soils*; ASAE: St. Joseph, MI, USA, 1971; ASAE Paper No. 190212.
92. de Moraes, M.T.; Gusmao, A.G. How do water, compaction and heat stresses affect soybean root elongation? A review. *Rhizosphere* **2021**, *19*, 100403. [CrossRef]
93. Souza, R.; Hartzell, S.; Ferraz, A.P.F.; de Almeida, A.Q.; de Sousa Lima, J.R.; Antonino, A.C.D.; de Souza, E.S. Dynamics of soil penetration resistance in water-controlled environments. *Soil Tillage Res.* **2021**, *205*, 104768. [CrossRef]
94. McCarter, W.J. The electrical resistivity characteristics of compacted clays. *Géotechnique* **1984**, *34*, 263–267. [CrossRef]
95. Molin, J.P.; Rabello, L.M. Studies on the measurement of soil electrical conductivity. *Eng. Agrícola* **2011**, *31*, 90–101. [CrossRef]
96. Kurtuluş, C.; Yeken, T.; Durdağ, D. Estimating the soil water content using electrical conductivity, oven method and speedy moisture tester. *Eurasian Soil Sci.* **2019**, *52*, 1577–1582. [CrossRef]
97. Mirzakhaninafchi, H.; Mishra, I.M.; Nafchi, A.M. Study on soil nitrogen and electrical conductivity relationship for site-specific nitrogen application. In Proceedings of the ASABE Annual International Meeting, Spokane, WA, USA, 16–19 July 2017; p. 1. [CrossRef]

98. Chung, S.O.; Sudduth, K.A.; Hummel, J.W. Design and validation of an on-the-go soil strength profile sensor. *Trans. ASABE* **2006**, *49*, 5–14. [CrossRef]
99. Calamita, G.; Brocca, L.; Perrone, A.; Piscitelli, S.; Lapenna, V.; Melone, F.; Moramarco, T. Electrical resistivity and TDR methods for soil moisture estimation in central Italy test-sites. *J. Hydrol.* **2012**, *454*, 101–112. [CrossRef]
100. Ansari, S.; Norooz, R.; Zeynolabedin, A.; Foadi, H.; Ghiassi, R. Experimental investigation of correlations between electrical resistivity, moisture content and voltage values for leachate contaminated clayey sand. *J. Appl. Geophys.* **2021**, *193*, 104391. [CrossRef]
101. Duan, Z.; Yan, X.; Sun, Q.; Tan, X.; Dong, C. Effects of water content and salt content on electrical resistivity of loess. *Environ. Earth Sci.* **2021**, *80*, 469. [CrossRef]
102. Fagbemigun, S.T.; Oyebamiji, R.A.; Faluyo, I.J.; Arowoogun, I.K.; Amosun, O.J.; Sanuade, A.O. Integration of electrical resistivity and soil analysis for agricultural soil characterization—A case study. *Arab. J. Geosci.* **2021**, *14*, 377. [CrossRef]
103. Han, Y.; Che, A.; Feng, S. A system and analytical method for testing the electrical parameters of soil. *Transp. Saf. Environ.* **2021**, *3*, 57–71. [CrossRef]
104. Ganiyu, S.A.; Olurin, O.T.; Oladunjoye, M.A.; Badmus, B.S. Investigation of soil moisture content over a cultivated farmland in Abeokuta, Nigeria using electrical resistivity methods and soil analysis. *J. King Saud-Univ.-Sci.* **2020**, *32*, 811–821. [CrossRef]
105. Friedman, S.P. Soil properties influencing apparent electrical conductivity: A review. *Comput. Electron. Agric.* **2005**, *46*, 45–70. [CrossRef]
106. Oussible, M.; Allmaras, R.R.; Wynch, R.D.; Crookston, R.K. Subsurface compaction effects on tillering and nitrogen accumulation in wheat. *Agron. J.* **1993**, *85*, 619–625. [CrossRef]
107. Potocka, I.; Szymanowska-Pułka, J. Morphological responses of plant roots to mechanical stress. *Ann. Bot.* **2018**, *122*, 711–723. [CrossRef]
108. Kobaissi, A.N.; Kanso, A.A.; Kanbar, H.J.; Kazpard, V.A. Morpho-physiological changes caused by soil compaction and irrigation on *Zea mays*. *Eurasian J. Soil Sci.* **2013**, *2*, 114–121.
109. Roberts, J.A.; Hussain, A.; Taylor, I.B.; Black, C.R. Use of mutants to study long-distance signalling in response to compacted soil. *J. Exp. Bot.* **2002**, *53*, 45–50. [CrossRef]
110. Peixoto, D.S.; Silva, B.M.; Godinho Silva, S.H.; Karlen, D.L.; Moreira, S.G.; Pereira da Silva, A.A.; Vilela de Resende, Á.; Norton, L.D.; Curi, N. Diagnosing, ameliorating, and monitoring soil compaction in no-till Brazilian soils. *Agrosystems Geosci. Environ.* **2019**, *2*, 1–14. [CrossRef]
111. Pott, L.P.; Amado, T.J.; Leal, O.A.; Ciampitti, I.A. Mitigation of soil compaction for boosting crop productivity at varying yield environments in southern Brazil. *Eur. J. Soil Sci.* **2020**, *71*, 1157–1172. [CrossRef]
112. Serrano, J.M.; Shahidian, S.; Marques da Silva, J. Spatial variability and temporal stability of apparent soil electrical conductivity in a Mediterranean pasture. *Precis. Agric.* **2017**, *18*, 245–263. [CrossRef]

Disclaimer/Publisher's Note: The statements, opinions and data contained in all publications are solely those of the individual author(s) and contributor(s) and not of MDPI and/or the editor(s). MDPI and/or the editor(s) disclaim responsibility for any injury to people or property resulting from any ideas, methods, instructions or products referred to in the content.